Synthesis and Characterization of $CoFe_2O_4/(SiO_2 - CaO - P_2O_5)$ Magnetic Bioactive Glass Nanoparticles for Biomedical Applications

Thenmozhi T., Ashina Nazar N., Savitha Pillai S. *

Department of Physics, University of Kerala, Thiruvananthapuram, Kerala PIN 695581, India

Editor's note: Magnetic bioactive glass nanoparticles (MBGs) are a promising system for targeted biomedical applications, such as bone regeneration and controlled drug delivery. Thenmozhi T. et al. synthesized MBGs composed of 60% SiO_2, 36% CaO, and 4% P_2O_5, with the addition of $CoFe_2O_4$ at concentrations of 2% (MBG2) and 4% (MBG4) for biomedical applications. Structural analysis revealed that MBG4 exhibited a 50% increase in UV absorption and a higher saturation magnetization compared to MBG2. These results suggest that incorporating up to 4% $CoFe_2O_4$ enhances the properties of MBGs for targeted therapies and magnetic hyperthermia.

doi: 10.22034/jams.2026.260302

How to cite: T. T. et al., *Journal of Applied Material Science*, **2026**, 2, 260302.

JOURNAL OF
APPLIED
MATERIAL
SCIENCE
jams.hsu.ac.ir

Journal of Applied Material Science **2026**, *2*, 260302
How to cite: T. T. et al., *Journal of Applied Material Science*, **2026**, *2*, 260302.
Journal homepage: **jams.hsu.ac.ir**

Original Research

Synthesis and Characterization of $CoFe_2O_4/(SiO_2 - CaO - P_2O_5)$ Magnetic Bioactive Glass Nanoparticles for Biomedical Applications

Thenmozhi T., Ashina Nazar N., Savitha Pillai S. *

Department of Physics, University of Kerala, Thiruvananthapuram, Kerala PIN 695581, India

Abstract

Magnetic bioactive glass nanoparticles are emerging as an effective multifunctional system for targeted biomedical applications, including bone regeneration, controlled drug delivery, and magnetic hyperthermia therapy. In this study, magnetic bioactive glass (MBG) nanoparticles with a nominal composition of $60SiO_2$-$36CaO$-$4P_2O_5$ (mol%) were synthesized by incorporating $CoFe_2O_4$ nanoparticles as the magnetic phase. The MBG nanoparticles were prepared using the sol–gel method, whereas $CoFe_2O_4$ nanoparticles were synthesized via the solvothermal method. The magnetic phase was introduced into the glass matrix at concentrations of 2% (MBG2) and 4% (MBG4). Structural characterizations were conducted using X-ray Diffraction (XRD) and Fourier Transform Infrared Spectroscopy (FTIR), confirming the presence of $CoFe_2O_4$ in the glass matrix. Morphological analysis was performed using Field Emission Scanning Electron Microscopy (FESEM), which validated the successful adsorption of $CoFe_2O_4$ nanoparticles into the bioactive glass. UV-Visible spectroscopy revealed a substantial change in the optical absorption behavior of the glass upon the addition of $CoFe_2O_4$. In particular, the MBG4 sample showed a nearly 50% increase in UV absorption compared to bare glass. Zeta potential measurements indicated that both MBG2 and MBG4 exhibit high colloidal stability, with significantly improved dispersion behavior compared with the pure bioactive glass. Magnetic measurements demonstrated that MBG4 exhibits a markedly higher saturation magnetization than MBG2. From the overall results, the incorporation of $CoFe_2O_4$ up to 4% was identified as the optimal concentration for the selected glass composition. The combined improvements in optical, colloidal, and magnetic properties highlight the potential of magnetic bioactive glass nanoparticles for biomedical applications, particularly in targeted therapy and magnetic hyperthermia.

Keywords: Magnetic bioactive glass nanoparticles; Cobalt ferrites; Magnetic hyperthermia.

1. Introduction

Bioactive glass nanoparticles are silicate-based materials, typically composed of $60SiO_2$–$36CaO$–$4P_2O_5$ (mol%), closely resembling bone hydroxyapatite [1]. The SiO_2–CaO–P_2O_5 system is well known for its excellent bioactivity due to its ability to form a hydroxyapatite layer in physiological environments, supporting bone bonding and regeneration [2]. These materials release

* Corresponding author.
Email address: savitha@keralauniversity.ac.in (S.P. Suseela)

Received 21 February 2026
Revised 5 June 2026
Accepted 21 June 2026
Available online 7 July 2026

https://doi.org/10.22034/jams.2026.260302

biologically active ions such as Ca^{2+}, PO_4^{3-}, and Si^{4+}, which stimulate cellular responses and promote tissue regeneration [3]. When combined with magnetic components, bioactive glass nanoparticles can enable applications such as medical imaging and magnetic hyperthermia, providing localized heat for cancer treatment while supporting tissue regeneration [4, 5].

The selection of synthesis methods plays a critical role in determining the structural and functional properties of the developed system. Bioactive glass nanoparticles can be synthesized using various methods, including sol–gel processing, melt-quenching [6], and microemulsion techniques [7]. In this study, the sol–gel method was employed for the synthesis of bioactive glass due to its ability to provide molecular-level homogeneity, precise compositional control, and high surface area, all of which are essential for enhanced bioactivity and rapid ion release.

Recent research on sol–gel-derived bioactive glass nanoparticles has focused on compositional tailoring through multi-ion doping to enhance bioactivity and biological performance. For instance, Bahati et al. (2023) demonstrated that strontium-doped systems exhibit improved apatite formation and enhanced bone regeneration potential [8]. Similarly, Miola et al. (2023) reported that co-doping with elements such as boron and copper enables the formation of spherical, monodispersed nanoparticles with enhanced biofunctional properties [9]. In another study, Cao et al. (2023) showed that zinc-doped bioactive glass nanoparticles possess significant antibacterial activity and can inhibit matrix metalloproteinases, thereby improving tissue adhesion, particularly in dental applications [10]. In addition, sol–gel-derived bioactive glasses have been explored for hyperthermia-based cancer treatment, highlighting their potential as multifunctional therapeutic systems. Borges et al. demonstrated the development of sol–gel-derived magnetic bioactive glass-ceramics containing superparamagnetic phases for effective hyperthermia applications [11]. Similarly, Nitu et al. reported enhanced induction heating efficiency in sol–gel-derived bioactive glass systems through the incorporation of magnetic nanoparticles [12]. Furthermore, recent studies have shown that sol–gel-synthesized magnetic bioactive glass nanoparticles exhibit combined bioactivity and hyperthermia functionality for biomedical applications [13].

Overall, these advancements indicate a shift toward highly engineered, multifunctional nanoscale bioactive glass systems with improved therapeutic efficiency and targeted clinical performance. Previous studies have demonstrated rapid apatite layer formation in simulated body fluid, confirming strong bioactivity, while also highlighting that synthesis parameters such as precursor composition, pH, and heat treatment conditions significantly influence particle size, porosity, surface area, and ion release behavior, thereby affecting the overall bioactivity and therapeutic performance of the material [1, 2, 8, 9].

Magnetic nanoparticles have emerged as promising agents for magnetic hyperthermia due to their unique properties such as superparamagnetism, high magnetization, and rapid magnetic response [14, 15]. Their nanoscale dimensions enable interaction with cellular components and the conversion of external magnetic fields into localized thermal or mechanical stimuli, allowing precise remote control of biological processes [16]. Among various MNPs, cobalt ferrite ($CoFe_2O_4$) is an attractive magnetic nanoparticle due to its strong magnetic properties, high chemical stability, high magnetic anisotropy, and relatively high Curie temperature (~520 °C). At the nanoscale, it exhibits semiconducting and superparamagnetic behavior, enabling efficient heat generation under an alternating magnetic field for hyperthermia applications [17]. In addition to magnetic hyperthermia, $CoFe_2O_4$ nanoparticles have been widely explored for applications in MRI contrast imaging, targeted drug delivery, and biosensing, highlighting their potential as multifunctional materials suitable for integration with bioactive systems [18].

In this work, the solvothermal method was selected for the synthesis of cobalt ferrite nanoparticles due to its ability to provide precise control over particle size and morphology [19, 20]. Additionally, solvothermal synthesis is a cost-effective, environmentally friendly, and reliable method for preparing cobalt ferrite nanoparticles for magnetic and biomedical applications, as it is conducted in an aqueous medium without the use of toxic solvents [21, 22]. Although cobalt ferrite ($CoFe_2O_4$) nanoparticles exhibit excellent magnetic properties for hyperthermia applications [23], their direct biomedical use is limited by several challenges reported in recent studies, including particle agglomeration caused by strong magnetic dipole–dipole interactions [24], poor colloidal stability, and potential cytotoxicity associated with cobalt ion release [25]. In addition, difficulties in achieving controlled heat generation under alternating magnetic fields have also been reported [26].

Recent studies have highlighted the importance of surface modification or matrix incorporation to improve nanoparticle stability, biocompatibility, and therapeutic performance [27]. To overcome these limitations, the incorporation of $CoFe_2O_4$ nanoparticles into a bioactive glass matrix has emerged as an effective strategy for improving particle dispersion, structural stability, and controlled thermal response [28]. Furthermore, the bioactive glass matrix enhances bioactivity and supports tissue regeneration, making magnetic bioactive glass composites promising multifunctional materials for biomedical applications [29].

Recent studies have increasingly focused on the development of multifunctional bioactive glass nanoparticle systems for combined therapeutic and regenerative applications. Valverde et al. reported that magnetic Fe_3O_4 nanoparticles coated with bioactive glass–naproxen exhibit enhanced bioactivity, improved surface functionality, and promising in vitro biomedical performance [30]. Similarly, Vishwakarma and Sinha explored additively manufactured magnetic bioactive glass scaffolds, demonstrating their potential in bone tissue engineering and drug delivery through optimized structural design [31]. In addition, Chen et al. highlighted recent advances in multifunctional bioactive glass nanoparticles, particularly emphasizing surface engineering strategies to improve bioimaging, tumor therapy, and tissue regeneration [32]. These studies collectively demonstrate the growing interest in integrating bioactive and magnetic functionalities into a single material system for advanced biomedical applications.

Bioactive glass nanoparticles are widely recognized for their excellent bone regeneration and tissue repair capabilities, while cobalt ferrite ($CoFe_2O_4$) nanoparticles are well studied for magnetic hyperthermia applications. However, the integration of these two materials into a single multifunctional system remains limited, and their combined potential for simultaneous therapy and regeneration is not fully explored. Moreover, there is a lack of effective synthesis strategies that can ensure uniform incorporation of magnetic nanoparticles within a bioactive glass matrix while preserving both magnetic and bioactive properties. In this context, the present study addresses this gap by synthesizing cobalt ferrite–incorporated bioactive glass using the sol–gel method, aiming to achieve a balanced combination of magnetic response and bioactivity and to systematically investigate its structural characteristics, UV absorption behavior, colloidal stability, and magnetic properties. The developed material is designed to enable localized cancer treatment through magnetic hyperthermia while also supporting tissue regeneration. This work contributes to the emerging field of magnetic bioactive glasses and offers a promising approach toward minimally invasive, multifunctional biomaterials for future biomedical applications [33-35].

2. Experimental

2.1. Materials

Tetraethoxysilane (TEOS), triethyl phosphate (TEP), calcium nitrate ($Ca(NO_3)_2$), ethylene glycol, iron nitrate ($Fe(NO_3)_3$), cobalt nitrate ($Co(NO_3)_2$), ammonia solution, ethanol, and deionized water were all of analytical grade and used as received.

2.2. Synthesis of bioactive glass nanoparticles using the sol-gel method

Bioactive glass (BG) was synthesized via the Sol-gel method (Figure 1). The sol–gel method allows molecular-level homogeneity of bioactive glass nanoparticles, which is crucial for biomedical applications. This technique also operates at relatively low temperatures, reducing the risk of unwanted crystallization and enabling the incorporation of heat-sensitive dopants or therapeutic ions. Additionally, sol-gel produces nanoparticles with high surface area and porosity, enhancing bioactivity and ion release in body fluids.

Initially, Solution A was prepared by mixing 2.25 mL of tetraethyl orthosilicate (TEOS), 0.23 mL of triethyl phosphate (TEP), and 25 mL of ethanol, followed by stirring for 30 min. Separately, Solution B was prepared by mixing 4.5 mL of ammonia solution, 8.12 mL of ethanol, and 12.38 mL of distilled water, stirring for 30 min. Then, solution A was slowly added to solution B, and the mixture was stirred for 1 hour, during which a white colloidal sol formed within 2 minutes. Next, 1.45 g of calcium nitrate ($Ca(NO_3)_2$) was added to the sol and stirred for another 30 minutes. The bioactive glass nanoparticles are formed in this colloidal solution. The

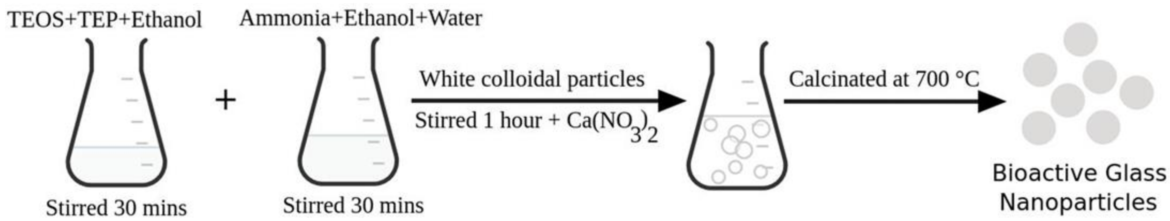

Figure 1. Sol-gel synthesis of BG.

resulting sol was centrifuged. The final precipitate was dried in a vacuum oven at 60°C for 6 h. The dried powder was then calcined in a muffle furnace at 700°C for 2 h at the rate of 2.34°C/min, yielding BG. This procedure is essential for removing nitrate ions and enabling the diffusion of calcium ions within the silica network [36].

2.3 Synthesis of Cobalt ferrite ($CoFe_2O_4$) using the solvothermal method

Cobalt Ferrite ($CoFe_2O_4$) nanoparticles were synthesized via the solvothermal method (Figure 2). Initially, 1.6 g of iron nitrate ($Fe(NO_3)_3$) and 0.575 g of cobalt nitrate ($Co(NO_3)_2$) were separately dissolved in 10 mL of ethylene glycol, sonicated for 20 minutes to ensure complete dissolution, mixed, and stirred at 70 °C for 30 min. 17.75 mL of ammonia solution was added, followed by stirring for another 30 min at 70 °C. The mixture was transferred to a Teflon-lined autoclave and subjected to solvothermal treatment at 180 °C for 4 hours. After cooling, the obtained product was centrifuged and vacuum-dried at 50°C for 5 h to obtain CoFe2O4 (CoF) nanoparticles [19].

2.4 Synthesis of Magnetic bioactive glass nanoparticles using the sol-gel method

Magnetic bioactive glass (MBG) was synthesized following the same Sol-gel procedure as BG till the addition of calcium nitrate ($Ca(NO_3)_2$) (see Figures 3 and 4). After the addition of 1.45 g of calcium nitrate ($Ca(NO_3)_2$) to the colloidal solution, the mixture was stirred for 30 min, followed by the introduction of cobalt ferrite ($CoFe_2O_4$) nanoparticles, which will be coated on the surface of the glass nanoparticles due to their adsorption property. Then, a measured amount of cobalt ferrite ($CoFe_2O_4$) was added, and the mixture was stirred for 1 h. The resulting mixtures were centrifuged, dried in a vacuum oven at 60°C for 6 h, and then calcinated in a muffle furnace at 700°C for 2 h. MBG samples containing 2 wt% and 4 wt% $CoFe_2O_4$ were synthesized and designated as MBG2 and MBG4, respectively [37]. During the synthesis process of MBG, it is necessary to make a colloidal solution of $CoFe_2O_4$ with the bioactive glass nanoparticle, and the resulting mixture will be in a dispersed state with no sign of $CoFe_2O_4$ particles settling down. When $CoFe_2O_4$ particles are added at levels above 4%, they settle and do not form a colloidal solution even after long-term sonication.

2.5. Measurements

X-ray diffraction (XRD) analysis was performed using a Bruker D8 ADVANCE with DAVINCI design for crystallinity and phase identification. The measurements were carried out in the 2θ range of 5°-120° using Cu Ka radiation, with a step size of 0.02° and a total scan time of 1 hour. The obtained diffraction data were analyzed using OriginPro software. Fourier transform infrared spectroscopy (FTIR) was performed using a Thermo Scientific Nicolet iS50 to determine

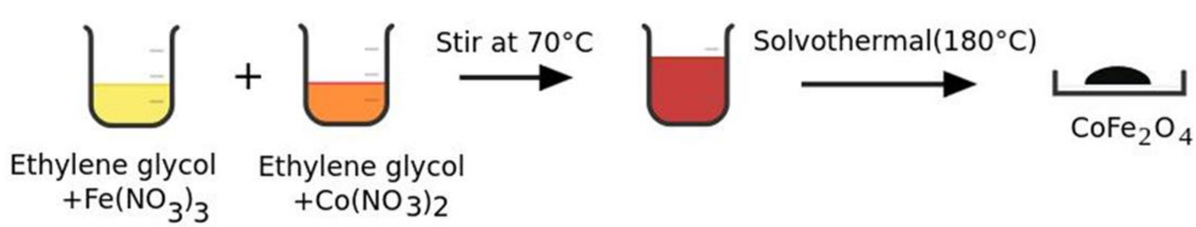

Figure 2. Preparation of $CoFe_2O_4$ by the Solvothermal method.

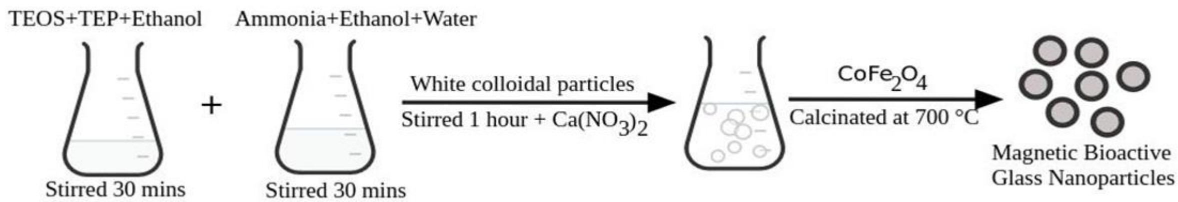

Figure 3. Sol-gel synthesis of MBG.

functional groups and bonding in the samples. UV–Visible Spectroscopy was performed using a JASCO V-750 UV–Visible Spectrophotometer with a wavelength range of 200-900 nm and 1 nm resolution. Field-emission scanning electron microscopy (FESEM) with a resolution of 100nm was performed to observe the microstructure and morphology. SEM images were analyzed using ImageJ software to determine the particle size of the samples. Hydrodynamic diameter and Zeta potential were studied using a Litesizer 500 (Anton Paar) instrument. The magnetic properties of 2% and 4% $CoFe_2O_4$-incorporated MBG samples were measured at 300K using Quantum Design Versalab PPMS under an applied magnetic field of 3T. The results were interpreted using OriginPro software.

3. Results and discussion

3.1. Structural analysis using X-ray diffractometers

XRD patterns of Cobalt Ferrite ($CoFe_2O_4$), its Rietveld-refined data, Bioactive glass (BG), and Magnetic Bioactive Glass (MBG) are shown in Figure 4a-d, respectively. From the XRD patterns of Bioactive Glass

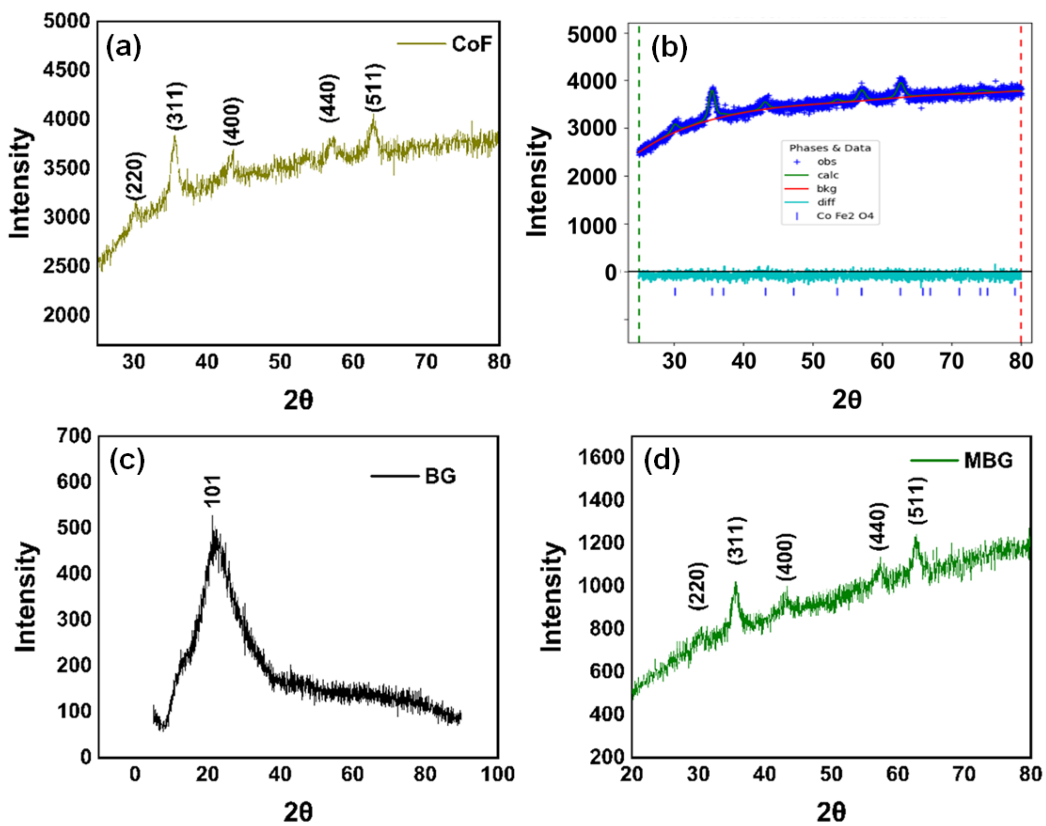

Figure 4. (a) XRD patterns of Cobalt Ferrite (CoFe2O4), (b) its Rietveld-refined data, (c) Bioactive glass (BG), and (d) Magnetic Bioactive Glass (MBG).

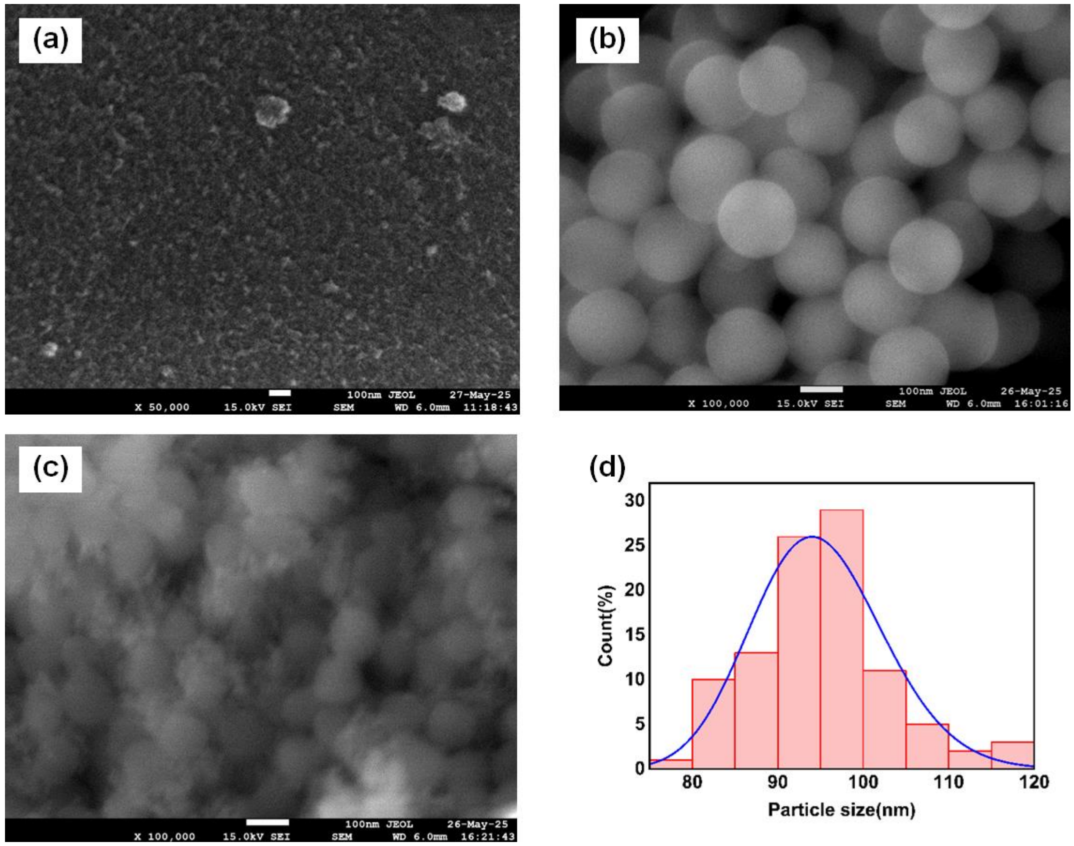

Figure 5. FESEM images of (a) $CoFe_2O_4$, (b) BG, (c) MBG, and (d) the particle distribution curve of BG.

with composition Silica (SiO_2), Calcium Oxide (CaO), and Phosphorus Pentoxide (P_2O_5) with a mol% ratio 15:9:1, a broad peak was observed at 2θ = 22.17°, which is characteristic of amorphous silicate materials, confirming the amorphous nature of the synthesized bioactive glass (BG). Additionally, the broad peak observed around 25° in the top diffraction pattern is attributed to the (101) planes in the amorphous silica structure.

For cobalt ferrite nanoparticles, the diffraction peaks were observed at 2θ angles of 30.4°, 35.5°, 43.2°, 53.6°, 57.1°, 62.7°, and 74.4°, which correspond to the (220), (311), (400), (422), (511), (440), and (533) planes, respectively. The average crystallite size was determined using the Scherrer equation: $D = K\lambda / \beta cos\theta$. The calculated crystallite size was approximately 13.3 nm. The presence of the characteristic diffraction peaks, particularly the (311) reflection, confirms the formation of the spinel structure of cobalt ferrite ($CoFe_2O_4$) [38]. For Magnetic Bioactive Glass, sharp diffraction peaks were observed at 2θ values of 30.42°, 35.67°, 43.49°, 57.21°, and 62.77°, corresponding to the (220), (311), (400), (511), and (440) crystal planes, respectively. These peaks are absent in BG and closely match the standard diffraction pattern of $CoFe_2O_4$, confirming the successful incorporation of the magnetic phase in the synthesized MBG. Table 1 shows the structural parameters of $CoFe_2O_4$ nanoparticles, which agree with previously reported values [39, 40].

3.2 Morphological Analysis

FESEM images were obtained to investigate the surface morphology and particle size of the synthesized bioactive glass (BG), cobalt ferrite nanoparticles, and

Table 1. Structural parameters of $CoFe_2O_4$ nanoparticles

Structural Parameters	**$CoFe_2O_4$**
Space Group	F d – 3 m
Unit Cell Parameter	8.43549
Cell Volume	600.249
Average Crystalline Size	13.3 nm

magnetic bioactive glass (MBG) nanoparticles. As shown in Figure 5, the BG nanoparticles exhibit a relatively uniform and spherical morphology with an average particle diameter of approximately 190 nm. The particle distribution curve of the FESEM image of BG is also depicted in the figure. The FESEM image of cobalt ferrite nanoparticles shows spherical, agglomerated particles. This agglomeration is attributed to the strong magnetic interactions and Van der Waals forces acting between the cobalt ferrite nanoparticles [41].

From the FESEM image of the MBG4 sample, it can be observed that the cobalt ferrite nanoparticles were adsorbed on the surface of the glass nanoparticles, while some were left behind without any change. These changes confirm the successful adsorption of glass nanoparticles and cobalt ferrite nanoparticles. Collectively, the ability of these bioactive glass nanoparticles to form layers on their surfaces and to resorb could enhance bioactivity, making them suitable for various biomedical applications [42].

3.3 FT-IR Spectroscopy Analysis

FTIR spectra of Bioactive Glass (BG) and Magnetic Bioactive Glass (MBG) nanoparticles are shown in Figure 6. In BG, the symmetric and asymmetric stretching vibrations of Si–O–Si are observed at 801 cm^{-1} and 1064 cm^{-1}, confirming the formation of the silicate network. Similarly, P-O stretching is observed at 1064 cm^{-1}, overlapping with Si-O-Si stretching, resulting in a broad spectrum between 871 and 1274 cm^{-1} [43]. In MBG nanoparticles, the Co–O stretching vibration is observed at 571 cm^{-1}, confirming the incorporation of magnetic cobalt species.

The symmetric and asymmetric stretching vibrations of Si–O–Si are located at 804 cm^{-1} and 1095 cm^{-1}, respectively. The shift of these bands compared to BG indicates the incorporation of $CoFe_2O_4$ into the silicate network, leading to increased bond strength and structural densification. The P–O stretching vibration is associated with the band at 1095 cm^{-1}, confirming that the fundamental bioactive glass network is preserved after magnetic phase incorporation [35].

3.4 UV – Visible Spectra

UV-Visible spectra of bioactive glass nanoparticles (BG) and Magnetic bioactive glass nanoparticles (MBGs) have been studied over the wavelength range of 200-900 nm. The BG, MBG2, and MBG4 samples were prepared at a concentration of 0.000125 g/mL. For the $CoFe_2O_4$ nanoparticles, the same initial concentration was used; however, only a weak absorbance peak was observed. Therefore, the concentration was increased to 0.00025 g/mL, and the experiment was repeated to better determine the position of the absorbance peak.

The BG sample shows negligible absorbance at about 246 nm. In contrast, the MBG samples show enhanced absorbance in the same wavelength region. The inset of Figure 7 shows the absorbance curve of $CoFe_2O_4$ nanoparticles, which shows absorbance at about 220 nm. $CoFe_2O_4$ shows significant absorbance in the UV region

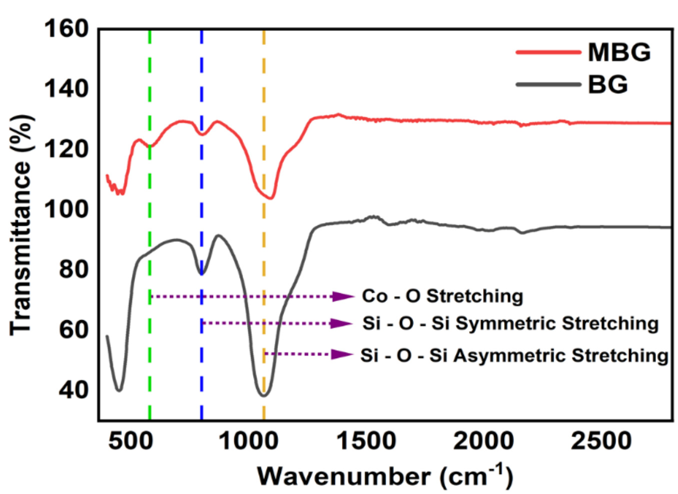

Figure 6. FTIR Spectra of BG and MBG.

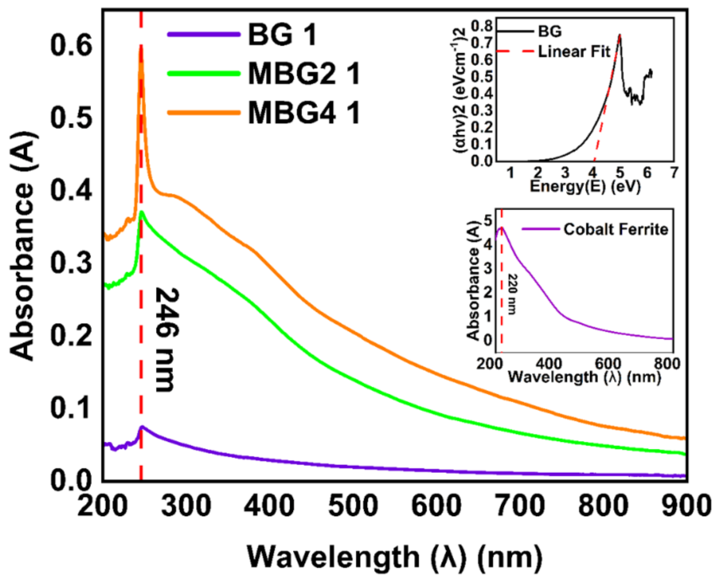

Figure 7. UV – Visible Spectra of BG, MBG2, and MBG4.

(200-400 nm), which contributes to the enhanced UV absorbance observed in the MBG samples containing $CoFe_2O_4$ [44].

The UV absorption of semiconducting cobalt ferrite nanoparticles arises from their electronic band structure. It is mainly caused by interband electronic transitions from the oxygen 2p valence band to the iron 3d conduction band. At the nanoscale, quantum confinement effects modify the band structure, altering the absorption behavior [19]. In the visible region (400–800 nm), broad absorption bands arise from electronic transitions within the cobalt d-orbitals. These transitions are influenced by the octahedral crystal field surrounding the cobalt ions, resulting in enhanced light absorption across the visible spectrum [45].

In silicate glass, optical absorption arises mainly from electronic transitions between the oxygen 2p valence band and silicon-related conduction band states. The observed ~50% increase in absorption in the magnetic glass composite can be attributed to the interfacial charge transfer from the wide-band-gap glass matrix to the $CoFe_2O_4$ nanoparticles. Because $CoFe_2O_4$ has lower-lying Fe 3d conduction-band states, electrons excited in the glass can transfer to the nanoparticles, introducing additional electronic transitions and thereby enhancing overall UV absorption. The absorbance increases with increasing $CoFe_2O_4$ nanoparticle concentration [46].

An increase in UV absorbance was observed in ferrite-doped bioactive glasses [47, 48]. The Tauc plot corresponding to the absorbance curve has been plotted. The band gap energy is obtained from the curve shown in the inset of Figure 7. From the Tauc plot of BG, shown in the figure, the band gap energy ranges from 3.8 to 4.2 eV, which agrees with previous studies [47]. Wider band gaps (>3 eV) promote biocompatibility by minimizing unwanted charge transfer or Reactive Oxygen Species (ROS) generation that could harm cells [49].

3.5 Dynamic Light Scattering (DLS) and Zeta Potential

DLS and Zeta Potential measurements were performed on all three samples to assess the Hydrodynamic Diameter and Colloidal Stability, respectively. As shown in Figure 8, the hydrodynamic diameters of BG, MBG2, and MBG4 are approximately 88 nm, 133.3 nm, and 97.7 nm, respectively. The corresponding Zeta Potential values are -25.7 mV, -46.3 mV, and -42 mV. The hydrodynamic diameter data indicate that most of the $CoFe_2O_4$ nanoparticles in MBG2 were adsorbed onto the surface of the bioactive glass nanoparticles, resulting in a larger particle size compared to BG. This observation is consistent with the FESEM analysis. Whereas the size of MBG4 is less than that of MBG2, which indicates that the surface of

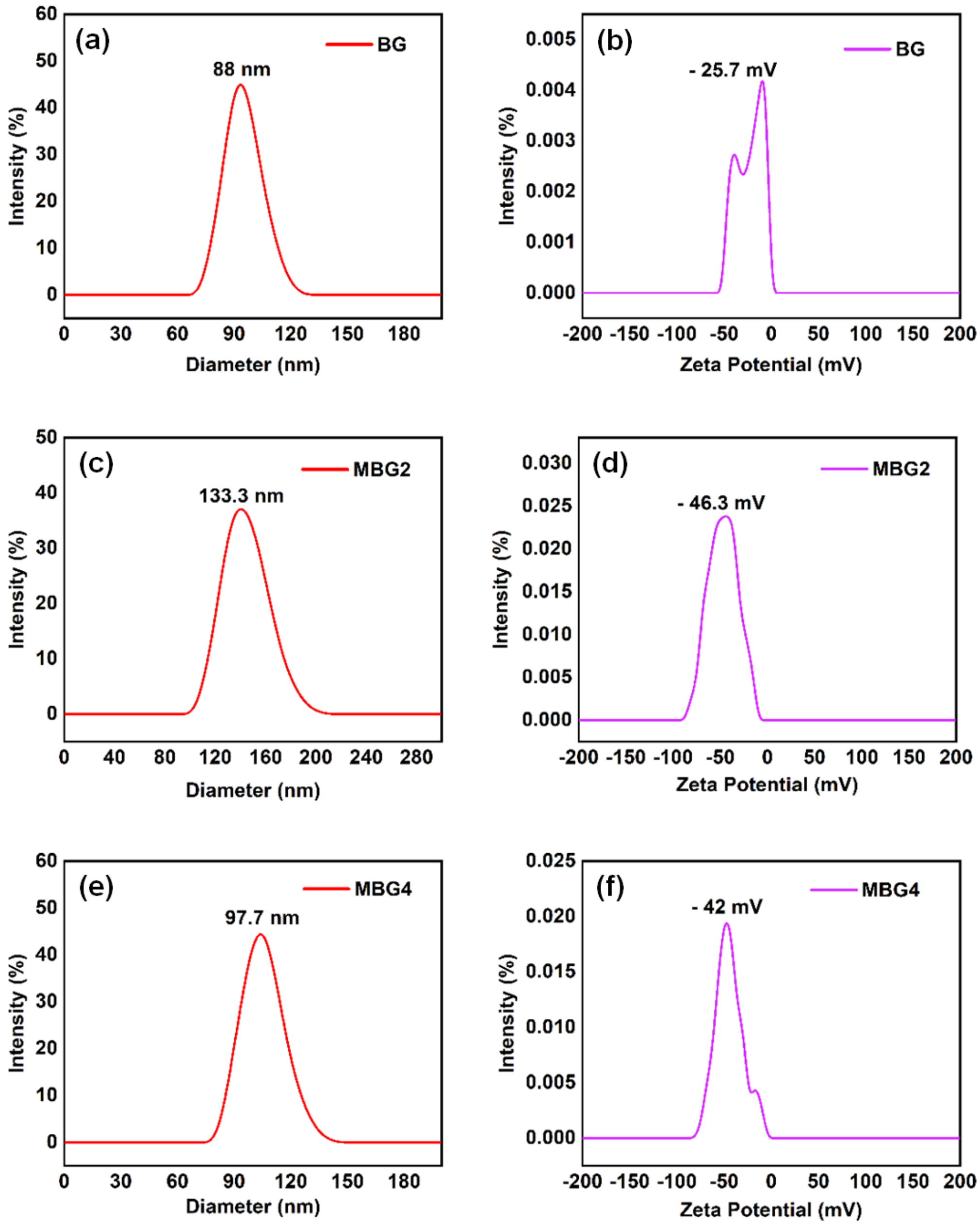

Figure 8. DLS and Zeta Potential curves of (a,b) BG, (c,d) MBG2, and (e,f) MBG4.

bioactive glass nanoparticles is not entirely covered with the $CoFe_2O_4$ nanoparticles.

During the synthesis of MBGs, it has been observed that the glass solution becomes saturated at about 4% addition of $CoFe_2O_4$ nanoparticles, above which the introduced $CoFe_2O_4$ nanoparticles do not mix with it. Zeta potential measurements reflect the surface charge and electrostatic potential of particles. In general, colloidal dispersions are considered stable when the zeta potential exceeds +30 mV or is lower than −30 mV. In our study, the measured zeta potential values indicate that the magnetic glasses are highly stable in suspension [50]. The results also reveal a clear dependence of zeta potential on composite size.

Variations in size change the relative number of surface atoms, which can influence properties such as

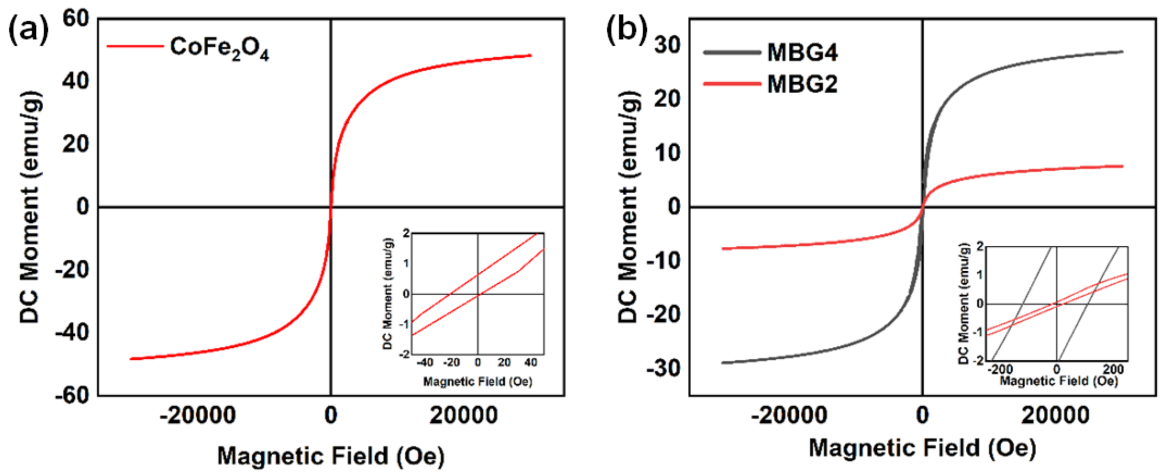

Figure 9. M-H Curves of (a) CoFe2O₄, as well as (b) BG, and MBG.

electronic structure, surface defect density, and porosity [51]. Comparing the Zeta potential values of these samples, we can deduce that the BG samples are colloidally unstable. The MBG2 and MBG4 samples show good colloidal stability along with negative surface potentials. In aqueous media, cobalt ferrite ($CoFe_2O_4$) nanoparticles acquire surface charge through protonation and deprotonation of surface hydroxyl groups (Co–OH). The degree of ionization of these groups determines the overall surface charge of the particles. At pH values above 6.9, the cobalt ferrite particles exhibit a negative surface charge [52]. Therefore, the presence of $CoFe_2O_4$ is likely responsible for the observed increase in the stability of magnetic glass.

3.6 Magnetic Properties

The field-dependent magnetization (M-H) curves of $CoFe_2O_4$ and Magnetic Bioactive Glass (MBG) with 2% and 4% $CoFe_2O_4$ incorporation are shown in Figure 9. The Magnetic saturation (M_S), Coercivity (H_C), and Remanence (M_R) values of the samples are listed in Table 2. It is observed that the coercivity value of $CoFe_2O_4$ is very low, and the crystalline size, as obtained from the XRD analysis, is around 13.3nm, which confirms the superparamagnetic nature of cobalt ferrite [53].

The saturation magnetism value of 4% $CoFe_2O_4$ MBG shows a drastic increase of about 11.23% when compared to 2% $CoFe_2O_4$ added MBG. From hydrodynamic size analysis, we confirmed that more $CoFe_2O_4$ nanoparticles were present on the surface of MBG2 than on MBG4, indicating that in MBG4, $CoFe_2O_4$ was not entirely concentrated at the surface of the glass nanoparticles, but remained as such. This may explain the drastic increase in the saturation magnetization of the MBG4 sample, due to the presence of free $CoFe_2O_4$ nanoparticles in the system. In the 2% CoFe2O4-added MBG sample, the glass nanoparticles are more prominent than the cobalt ferrite nanoparticles. In the 4% sample, the magnetic nanoparticles appear to have effectively occupied the space between the glass phases. This observation is supported by the scanning electron microscopy (SEM) image, which shows that the glass phase is not distinctly visible and appears cloud-like. The coercivity of MBGs increases as the addition of $CoFe_2O_4$ in the bioglass matrix increases. This trend arises from strong interparticle interactions as the magnetic phase concentration increases [54]. Within the superparamagnetic regime, the obtained coercivity

Table 2. Magnetic saturation, Coercivity, and Remanence values of samples

Sample	Magnetic saturation, Ms (emu/g)	Coercivity, HC (Oe)	Remanence, MR (emu/g)
$CoFe_2O_4$	48.29	9.645	0.64
MBG 2%	7.65	2.85	0.065
MBG 4%	28.88	6.515	2.4

values demonstrate favorable particle-heating properties. This observation suggests that these materials are strong candidates for hyperthermia applications [55].

4. Conclusions

In this study, MBG was synthesized by the sol-gel method, incorporating $CoFe_2O_4$ nanoparticles, which were synthesized via the solvothermal method, into a Bioactive glass (SiO_2–P_2O_5–CaO) matrix. The results demonstrated that the incorporation of $CoFe_2O_4$ nanoparticles significantly influenced the structural, morphological, optical, and magnetic properties of the material. Structural analysis with XRD confirmed the amorphous nature of BG and the formation of the spinel structure of the $CoFe_2O_4$ phase, while FTIR results marked the presence of Co-O vibration in the silicate network. From UV – Visible spectroscopy analysis, the MBG samples show increased absorbance due to the presence of $CoFe_2O_4$. Morphological studies revealed that most of the $CoFe_2O_4$ nanoparticles are adsorbed onto the glass surface, while a smaller fraction remains unbound and forms agglomerates. Hydrodynamic diameter analysis indicated that MBG2 had the greatest amount of $CoFe_2O_4$ attached to its surface. Both MBG2 and MBG4 samples exhibit good stability in water, as confirmed by a significant increase in their zeta potential values. Furthermore, the magnetic properties of MBG were strongly dependent on the $CoFe_2O_4$ concentration, with higher concentrations leading to increased saturation magnetization while maintaining low coercivity and superparamagnetic behavior. $CoFe_2O_4$ nanoparticles incorporated into bioactive glass significantly enhance UV absorption, improve colloidal stability, and impart magnetic properties. These properties enable efficient heat generation under an alternating magnetic field and optical imaging, both of which are essential for targeted magnetic hyperthermia applications aimed at destroying cancer cells. Simultaneously, the silicate-based bioactive glass matrix supports bone regeneration and ensures biocompatibility, making the material suitable for medical applications. Overall, this multifunctional magnetic glass material has significant potential to improve cancer treatment and help develop more effective medical therapies in the future.

Acknowledgments

The author, S. Savitha Pillai, would like to thank the University Grants Commission (UGC) and acknowledge the support from the Central Laboratory for Instrumentation and Facilitation (CLIF), University of Kerala.

Conflict of Interest

The authors declare no conflict of interest.

References

1. N. Pajares-Chamorro and X. Chatzistavrou. Bioactive Glass Nanoparticles for Tissue Regeneration. *ACS Omega*, 2020, *5*, 12716.
2. L. Hussein, et al. Advancements in mesoporous bioactive glasses for effective bone cancer therapy: Recent developments and future perspectives. *Biomaterials and Biosystems*, **2025**, *17*, 100108.
3. S. Safaee, et al. Effect of a novel bioactive glass synthesized by sol-gel method on restoring primary damage of enamel. *Next Materials*, **2025**, *8*, 100867.
4. F. Unal and B. Ercan. Magnetic and luminescence properties of bioactive glass nanoparticles for biomedical applications. *Journal of the Australian Ceramic Society*, **2024**, *61*, 301.
5. S.S. Danewalia and K. Singh. Bioactive glasses and glass–ceramics for hyperthermia treatment of cancer: state-of-art, challenges, and future perspectives. *Materials Today Bio*, **2021**, *10*, 100100.
6. H. Madival and A. Rajiv. A Comprehensive Review of Bioactive Glasses: Synthesis, Characterization, and Applications in Regenerative Medicine. *Biomedical Materials & Devices*, **2025**, *4*, 1380.
7. H. Wang, et al. Preparation and characterization of the system SiO2-CaO-P2O5 bioactive glasses by microemulsion approach. *Journal of Wuhan University of Technology-Mater. Sci. Ed.*, **2013**, *28*, 1053.
8. D. Bahati, M. Bricha, and K. El Mabrouk. Synthesis, characterization, and in vitro apatite formation of strontium-doped sol-gel-derived bioactive glass nanoparticles for bone regeneration applications. *Ceramics International*, **2023**, *49*, 23020.
9. M. Miola, et al. Sol-gel synthesis of spherical monodispersed bioactive glass nanoparticles co-doped with boron and copper. *Journal of Non-Crystalline Solids*, **2023**, *622*, 122653.

10. X. Cao, et al. Antibacterial and metalloproteinase-inhibited zinc-doped bioactive glass nanoparticles for enhancing dentin adhesion. *Journal of Dentistry*, **2025**, *154*, 105610.

11. R. Borges, et al. New sol-gel-derived magnetic bioactive glass-ceramics containing superparamagnetic hematite nanocrystals for hyperthermia application. *Materials Science and Engineering: C*, **2021**, *120*, 111692.

12. Nitu, et al. Enhancement in the induction heating efficacy of sol–gel derived SiO2–CaO–Na2O–P2O5 bioglass-ceramics by incorporating magnetite nanoparticles. *Journal of Materials Chemistry B*, **2024**, *12*, 3494.

13. C. Taşar and B. Ercan. Fabrication and biological properties of magnetic bioactive glass nanoparticles. *Ceramics International*, **2023**, *49*, 12925.

14. M.J. Ansari, et al. Synthesis and Stability of Magnetic Nanoparticles. *BioNanoScience*, **2022**, *12*, 627.

15. X. Yang, et al. Advances in magnetic nanoparticles for molecular medicine. *Chemical Communications*, **2025**, *61*, 3093.

16. M.S. Shakil, et al. Cobalt Ferrite Nanoparticle's Safety in Biomedical and Agricultural Applications: A Review of Recent Progress. *Current Medicinal Chemistry*, **2023**, *30*, 1756.

17. S.H. Patle, et al. A Comprehensive Review on synthesis, properties and applications of Cobalt Spinel Ferrites. *Foundry Journal*, **2024**, *27*, 117.

18. S.M. Ansari, et al. Cobalt ferrite nanoparticles: The physics, synthesis, properties, and applications. *Applied Physics Reviews*, **2025**, *12*.

19. N.M. Refat, M.Y. Nassar, and S.A. Sadeek. A controllable one-pot hydrothermal synthesis of spherical cobalt ferrite nanoparticles: synthesis, characterization, and optical properties. *RSC Advances*, **2022**, *12*, 25081.

20. M. Weißpflog, et al. Non-Stoichiometric Cobalt Ferrite Nanoparticles by Green Hydrothermal Synthesis and their Potential for Hyperthermia Applications. *The Journal of Physical Chemistry C*, **2024**, *128*, 15598.

21. A. Modabberasl, et al. Hydrothermal as a synthesis method for characterization of structural, morphological and magnetic properties of Co–Al ferrite nanoparticles. *Materials Chemistry and Physics*, **2024**, *314*, 128832.

22. J. Panda, et al. Investigation of antibacterial, antioxidant, and anticancer properties of hydrothermally synthesized cobalt ferrite nanoparticles. *Applied Physics A*, **2022**, *128*.

23. M.A. Medina, et al. Synthesis, Characterization and Magnetic Hyperthermia of Monodispersed Cobalt Ferrite Nanoparticles for Cancer Therapeutics. *Molecules*, **2020**, *25*, 4428.

24. D. Serantes and D. Baldomir. Nanoparticle Size Threshold for Magnetic Agglomeration and Associated Hyperthermia Performance. *Nanomaterials*, **2021**, *11*, 2786.

25. A.S. Garanina, et al. Cobalt Ferrite Nanoparticles for Tumor Therapy: Effective Heating versus Possible Toxicity. *Nanomaterials*, **2021**, *12*, 38.

26. I.S. Caizer and C. Caizer. Superparamagnetic Hyperthermia Study with Cobalt Ferrite Nanoparticles Covered with γ-Cyclodextrins by Computer Simulation for Application in Alternative Cancer Therapy. *International Journal of Molecular Sciences*, **2022**, *23*, 4350.

27. I. Baldea, et al. Magnetic Hyperthermia with Iron Oxide Nanoparticles: From Toxicity Challenges to Cancer Applications. *Nanomaterials*, **2025**, *15*, 1519.

28. F. Baino, M. Montazerian, and E. Verné. Cobalt-Doped Bioactive Glasses for Biomedical Applications: A Review. *Materials*, **2023**, *16*, 4994.

29. L. Zhang, et al. Recent advances in functionalized ferrite nanoparticles: From fundamentals to magnetic hyperthermia cancer therapy. *Colloids and Surfaces B: Biointerfaces*, **2024**, *234*, 113754.

30. T.M. Valverde, et al. Novel Fe3O4 Nanoparticles with Bioactive Glass–Naproxen Coating: Synthesis, Characterization, and In Vitro Evaluation of Bioactivity. *International Journal of Molecular Sciences*, **2024**, *25*, 4270.

31. A. Vishwakarma and N. Sinha. Determination of the Optimum Architecture of Additively Manufactured Magnetic Bioactive Glass Scaffolds for Bone Tissue Engineering and Drug-Delivery Applications. *ACS Applied Bio Materials*, **2024**, *7*, 6847.

32. M. Chen, et al. Multifunctional bioactive glass nanoparticles: surface–interface decoration and biomedical applications. *Regenerative Biomaterials*, **2024**, *11*, rbae110.

33. A. Manohar, et al. Synthesis, characterization and magnetic hyperthermia properties of nearly monodisperse CoFe2O4 nanoparticles. *Ceramics International*, **2020**, *46*, 28035.

34. B. Aslibeiki, et al. Magnetic hyperthermia properties of CoFe2O4 nanoparticles: Effect of polymer coating and interparticle interactions. *Ceramics International*, **2022**, *48*, 27995.

35. A.K. Yadav, et al. Synergistic effect of CoFe2O4–85S nano bio-glass composites for hyperthermia and controlled drug delivery. *Materialia*, **2023**, *32*, 101884.

36. C. Vichery and J.-M. Nedelec. Bioactive Glass Nanoparticles: From Synthesis to Materials Design for Biomedical Applications. *Materials*, **2016**, *9*, 288.

37. B.R. Barrioni, et al. The influence of cobalt incorporation and cobalt precursor selection on the structure and bioactivity of sol–gel-derived bioactive glass. *Journal of Sol-Gel Science and Technology*, **2018**, *88*, 309.

38. G. Katoch, et al. Crystal structure, synthesis, properties and potential applications of cobalt spinel ferrite: A brief review. *Materials Today: Proceedings*, **2023**, https://doi.org/10.1016/j.matpr.2023.03.585.

39. Y. Kumar, A. Sharma, and P.M. Shirage. Impact of different morphologies of CoFe2O4 nanoparticles for tuning of structural, optical and magnetic properties. *Journal of Alloys and Compounds*, **2019**, *778*, 398.

40. J. Xavier, et al. CoFe2O4@BiFeO3 core/shell nanoparticles: Synthesis, characterization, and fingerprints of the spin disorder. *Journal of Alloys and Compounds*, **2021**, *889*, 161650.

41. M. Yogesh Gopal. Physico-Chemical Characterization of Cobalt Ferrite Nano-Particles Synthesized Via Sol-Gel Method. *Educational Administration Theory and Practice*, **2024**, *30*, 3255.

42. P. Naruphontjirakul, P. Kanchanadumkerng, and P. Ruenraroengsak. Multifunctional Zn and Ag co-doped bioactive glass nanoparticles for bone therapeutic and regeneration. *Scientific Reports*, **2023**, *13*, 6775.

43. R. Bento, A. Gaddam, and J.M.F. Ferreira. Sol–Gel Synthesis and Characterization of a Quaternary Bioglass for Bone Regeneration and Tissue Engineering. *Materials*, **2021**, *14*, 4515.

44. T.K.C. Nguyen and A.T. Nguyen. Structural, optical and magnetic properties of Y-doped CoFe2O4 nanoparticles prepared by a simple co-precipitation method. *Journal of Materials Science: Materials in Electronics*, **2023**, *34*, 448.

45. H. Hussein, S.S. Ibrahim, and S.A. Khairy. Eco-friendly CoFe2O4 ferrite nanoparticles prepared using greek yogurt solution: deep insights into optical properties and abnormal semiconductor–insulator–semiconductor transitions for optoelectronics and catalytic applications. *Materials Advances*, **2025**, *6*, 2297.

46. U. Nurbaiti, et al. Optical properties of a low-temperature bioactive glass powders. *Journal of Physics: Conference Series*, **2021**, *1918*, 022006.

47. H.M.H. Zakaly, et al. Porous iron-doped bioactive glass nanoparticles: synthesis, detailed structural and optical analysis for advanced application in radiation shielding. *Journal of the Korean Ceramic Society*, **2025**, *62*, 1222.

48. F. Subhan, et al. Effective adsorptive performance of Fe3O4@SiO2 core shell spheres for methylene blue: kinetics, isotherm and mechanism. *Journal of Porous Materials*, **2019**, *26*, 1465.

49. A. Shafiee, et al. Energy Band Gap Investigation of Biomaterials: A Comprehensive Material Approach for Biocompatibility of Medical Electronic Devices. *Micromachines*, **2020**, *11*, 105.

50. P. Sennett and J.P. Olivier. Colloidal dispersions, electrokinetic effects, and the concept of zeta potential. *Industrial & Engineering Chemistry*, **1965**, *57*, 32.

51. M.R. Gittings and D.A. Saville. The determination of hydrodynamic size and zeta potential from electrophoretic mobility and light scattering measurements. *Colloids and Surfaces A: Physicochemical and Engineering Aspects*, **1998**, *141*, 111.

52. A. Zielińska-Jurek, et al. Design and Application of Magnetic Photocatalysts for Water Treatment. The Effect of Particle Charge on Surface Functionality. *Catalysts*, **2017**, *7*, 360.

53. G.M. Alzoubi, et al. Determination of critical size of superparamagnetism in as-prepared crystalline cobalt ferrite nanoparticles using magnetic measurements. *Applied Physics A*, **2025**, *131*, 623.

54. B. Aslibeiki, et al. Co-doped MnFe2O4 nanoparticles: magnetic anisotropy and interparticle interactions. *Beilstein Journal of Nanotechnology*, **2019**, *10*, 856.

55. F.H.L. Starsich, et al. Coercivity determines magnetic particle heating. *Advanced Healthcare Materials*, **2018**, *7*, 1800287.